Available online at www.sciencedirect.com
ScienceDirect
Journal of Computational Physics 225 (2007) 730–752
JOURNAL OF COMPUTATIONAL PHYSICS
www.elsevier.com/locate/jcp

An accurate elasto-plastic frictional tangential force–displacement model for granular-flow simulations: Displacement-driven formulation

Xiang Zhang [1], Loc Vu-Quoc *

Mechanical and Aerospace Engineering, University of Florida, Gainesville, FL 32611, USA

Received 7 August 2006; received in revised form 21 December 2006; accepted 22 December 2006
Available online 16 February 2007

Abstract

We present in this paper the displacement-driven version of a tangential force–displacement (TFD) model that accounts for both elastic and plastic deformations together with interfacial friction occurring in collisions of spherical particles. This elasto-plastic frictional TFD model, with its force-driven version presented in [L. Vu-Quoc, L. Lesburg, X. Zhang. An accurate tangential force–displacement model for granular-flow simulations: contacting spheres with plastic deformation, force-driven formulation, Journal of Computational Physics 196(1) (2004) 298–326], is consistent with the elasto-plastic frictional normal force–displacement (NFD) model presented in [L. Vu-Quoc, X. Zhang. An elasto-plastic contact force–displacement model in the normal direction: displacement-driven version, Proceedings of the Royal Society of London, Series A 455 (1991) 4013–4044]. Both the NFD model and the present TFD model are based on the concept of additive decomposition of the radius of contact area into an elastic part and a plastic part. The effect of permanent indentation after impact is represented by a correction to the radius of curvature. The effect of material softening due to plastic flow is represented by a correction to the elastic moduli. The proposed TFD model is accurate, and is validated against nonlinear finite element analyses involving plastic flows in both the loading and unloading conditions. The proposed consistent displacement-driven, elasto-plastic NFD and TFD models are designed for implementation in computer codes using the discrete-element method (DEM) for granular-flow simulations. The model is shown to be accurate and is validated against nonlinear elasto-plastic finite-element analysis.

Keywords: Granular flow simulation; Contact mechanics; Discrete-element method; Tangential force–displacement relation; Elastoplasticity; Frictional contact

* Corresponding author. Tel.: +1 352 392 6227; fax: +1 352 392 7303.
E-mail address: vu-quoc@ufl.edu (L. Vu-Quoc).
URL: http//www.mae.ufl.edu/~vql (L. Vu-Quoc).
[1] Now with Siemens Corporate Research, 755 College Road East, Princeton, NJ 08540, USA.

0021-9991/$ - see front matter
doi:10.1016/j.jcp.2006.12.028

1. Introduction and literature review

Particle systems in motion known as granular flows in nature and in industry have important implications that impact the safety and the economy of many human communities. Some examples are rock and snow avalanches (e.g. [3–5]), landslides (e.g. [6]), volcanic pyroclastic flows (e.g. [7]), submarine flows (e.g. [8]), pharmaceutical processing of medicine tablets (e.g. [9]). Even the mysterious songs[2] of sand dunes in deserts from the Gobi to the Death Valley, observed but unexplainable for almost 13 centuries, can now be explained as a result of sand (granular) flow (e.g. [11–13,13]). The readers are referred to [1] for a motivation on the need to model the inelastic nature of interparticle collisions and additional literature review.

Because of the limitation of conventional experimental measurements and the development of computer power, the discrete element method (DEM), as a computer simulation method, has been widely employed to study the flow behavior of granular materials in the last decade. Simulation results, complemented with experimental results when possible, were used to develop constitutive laws for granular flows in specifically different regimes (e.g. [14]). In DEM simulations, particles move as rigid bodies whose translational and rotational motions are governed by Newton's laws. During contacts, among the flowing particles, the contact forces are evaluated from the computed overlaps among those colliding particles using contact force–displacement (FD) models in both normal and tangential directions. The readers are referred to [15] for more details on DEM simulation procedure: contact detection, contact force evaluation, data structure, integration algorithms and numerical examples. Other applications of particle contact mechanics and DEM simulations can be found, e.g., in [16–23].

Accurate and efficient evaluation of the contact forces is crucial for a correct simulation of granular flows. More accurate elasto-plastic NFD model led to more accurate velocity-dependent coefficient of restitution, which is constant in some NFD model [24]. It has been amply demonstrated in [25] that improving the accuracy of the TFD model led to starkly different statistics of collision when compared to less accurate model. In addition, to the best of our knowledge, there has been in the literature no coherent set of normal force–displacement (NFD) and tangential force–displacement (TFD) models that can account for both elastic and plastic deformations at contact, together with interfacial friction, in a consistent manner.

For dry granular flows, particle–particle forces are mainly direct mechanical contact forces among the colliding particles. At a contact point, there are two contact forces: the normal contact force P, which acts in the direction normal to the contact plane, and the tangential force Q, which acts in the direction that lies in the contact plane. Fig. 1 features two spheres in contact, with contact plane (x, y), subjected to both normal force P and frictional tangential force Q. A NFD model gives the normal force P for a given normal displacement $\alpha = \frac{1}{2}(\alpha_i + \alpha_j)$,[3] whereas a TFD model gives the tangential force Q for a given tangential displacement $\delta = \frac{1}{2}(\delta_i + \delta_j)$.

We presented the force-driven version of an accurate and efficient elasto-plastic NFD model in [26], and then the displacement-driven version in [2]; this elasto-plastic NFD model has been experimentally validated in [27] based on detailed scanning electron microscopy and atomic force microscopy in a study on the mechanical and electrical behaviors of particulate polymer granular materials. Subsequently, in a follow-up work in [1], we presented the force-driven version of the elasto-plastic TFD model that is consistent with the formalism set forth in our previous work on the elasto-plastic NFD model, and consistent with the Hertz, Cattaneo, Mindlin, and Deresiewicz theory for frictional elastic contact. For implementation in DEM codes, it is important to develop the displacement-driven version, which is presented here.

We recall that the novelty of the present TFD model lies in (i) the additive decomposition of the elasto-plastic contact-area radius into an elastic part and a plastic part, (ii) the correction of the radii of the colliding particles at the contact point, and (iii) the correction of the elastic moduli of the colliding particles. The

[2] A low-pitch sound that was compared to that emitted by an airplane engine and an organ. The readers can listen to the actual sand-dune songs by going to the web site mentioned in [10].

[3] Even though α is the standard notation for the relative approach of distant points, it is more convenient to use 2α to describe the same quantity in our work.

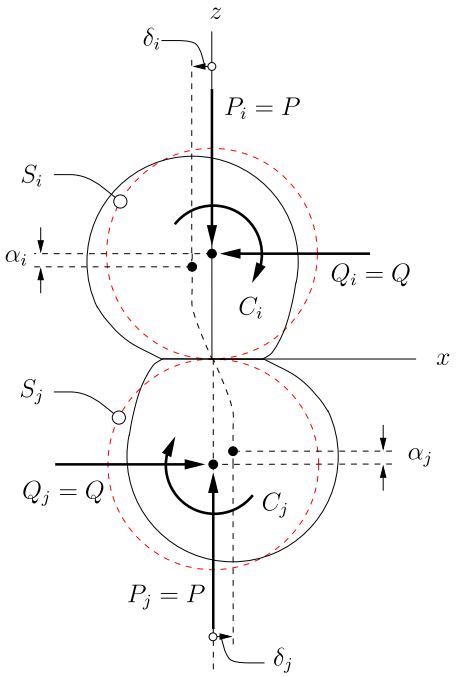

Fig. 1. Two spheres in contact: normal and tangential forces.

correction of the contact-area radius represents an effect of the plastic deformation in the colliding particles, whereas the correction of the radius of curvature represents a permanent indentation after impact. The correction of the elastic moduli represents a softening of the material due to plastic flow. The present displacement-version of the elasto-plastic-frictional TFD model is accurate, and is validated against nonlinear finite element analyses involving plastic flows under both loading and unloading conditions.

Below, we review briefly the theory of elastic contact and the various FD models employed in DEM simulations, in particular the elasto-plastic NFD model in [2] to set the stage to introduce the present elasto-plastic-frictional TFD model.

1.1. Theories for elastic contact

Hertz theory [28,29] provides the theoretical solution of the elastic contact between two homogeneous spheres in the normal direction. Most NFD models currently used in DEM simulations are based on Hertz theory of normal contact. Usually, the TFD model employed with a NFD model is based on Mindlin–Deresiewicz (MD) contact mechanics theory [30] for elastic frictional contact in the tangential direction between two homogeneous spheres. The MD contact theory [30] is a fundamental advance toward solving the problem of tangential elastic frictional contact. Both Hertz theory and MD theory [30] are accurate for elastic contact between two homogeneous spheres only when the radius of contact area is very small compared to the radii of the spheres; see [31] for finite element analysis (FEA) results. Even though, the theoretical solution from MD theory [30] is limited to *simple loading* histories (see also [32–34]), most of the TFD models currently used in DEM simulations are highly simplified models based on MD theory [30] (e.g. [32,35]), and are applied to all the loading histories encountered in granular flows. In addition, when using NFD models based on Hertz theory and TFD models based on MD theory [30] in DEM simulations, only elastic deformation is accounted for. Plastic deformation, which is not accounted for by many existing FD models occurs, however, in most particle collisions, as manifested through a coefficient of restitution less than one, and greatly affects the behavior of granular flows. Therefore, to obtain reliable and accurate simulation results, it is necessary to develop NFD and TFD models that account for both elastic and plastic deformation. See also [25] regarding the importance of more accurate FD models.

1.2. Walton & Braun [1986] NFD and TFD models for DEM simulations

NFD models based on Hertz theory give a nonlinear elastic relationship between the normal displacement α and the normal contact force P. Consequently, when simulating the collision between a sphere and a rigid half space, the ratio of outgoing velocity to the incoming velocity of the sphere, i.e., the coefficient of restitution, is $e = 1.0$, implying that there is no kinetic energy dissipation caused by the collision. For most of collision problems encountered in granular flows, plastic deformation occurs at contact points, resulting in a coefficient of restitution less than one, i.e., $e < 1$, as kinetic energy is dissipated after contact. To account for the effect of plastic deformation, Walton & Braun (WB) [35] proposed a bilinear FD model that provides a rough approximation to finite element analysis results [36] for elasto-plastic contact between a sphere and a rigid planar surface.

In the NFD model of WB [35], we have

$$P = \begin{cases} K_1\alpha & \text{for loading,} \\ K_2(\alpha - \alpha_0) & \text{for unloading,} \end{cases} \tag{1.1}$$

where P is the normal contact force between two particles, α the normal displacement (half of the relative displacement of the centers of the two spheres), K_1 and K_2 the slopes of the straight lines representing the loading and unloading stiffness coefficients, α_0 the residual displacement after complete unloading.

It can be proved that the coefficient of restitution e is related to the stiffness coefficients K_1 and K_2 as follows:

$$e = \sqrt{\frac{K_1}{K_2}}. \tag{1.2}$$

In a simulation, loading stiffness K_1 and unloading stiffness K_2 are constants for spheres, and usually $K_1 < K_2$. Therefore, the coefficient of restitution e from the NFD model of WB [35] is a constant less than one ($e < 1.0$) for a collision between two spheres. Even though the energy dissipation caused by plastic deformation is represented in this model, a constant coefficient of restitution does *not* agree with experimental evidence, since the coefficient of restitution does not depend only on the material properties, but also on the magnitude of the incoming velocity, and thus on the amount of plastic deformation in a collision (see [37–39]).

The TFD model of WB in [35], which is used with their proposed NFD model described above, is expressed as follows

$$Q_{n+1} = Q_n + K_{\mathrm{T},n}\Delta\delta_n, \tag{1.3}$$

where Q_{n+1} and Q_n are respectively the tangential force at time t_{n+1} and time t_n, $K_{\mathrm{T},n}$ the tangential stiffness coefficient at time t_n, and $\Delta\delta_n$ the incremental tangential displacement at time t_n, computed based on the motion of particles in the previous time step. The tangential stiffness $K_{\mathrm{T},n}$ is a function of P_n, Q_n, and Q^*, which is the value of the tangential force Q at the last turning point on the loading history of Q, and is expressed as follows [35]:

$$K_{\mathrm{T},n} = \begin{cases} K_{\mathrm{T},0}\left(1 - \dfrac{Q_n - Q^*}{\mu P_n - Q^*}\right)^{1/3} & \text{for } Q \text{ increasing } (\nearrow), \\ K_{\mathrm{T},0}\left(1 - \dfrac{Q^* - Q_n}{\mu P_n + Q^*}\right)^{1/3} & \text{for } Q \text{ decreasing } (\searrow), \end{cases} \tag{1.4}$$

where $K_{\mathrm{T},0}$ is the initial tangential stiffness computed following relation (1.5), and μ the friction coefficient. For initial loading, Q^* is set to zero. The value of Q^* will be subsequently reset to the value of Q at the turning points, i.e., where the magnitude of the tangential force Q changes from increasing to decreasing, or vice versa. The initial tangential stiffness $K_{\mathrm{T},0}$ is connected to the normal stiffness K_1 as [29, p. 220; 30, p.327]

$$K_{\mathrm{T},0} = K_1\frac{2(1-\nu)}{2-\nu}, \tag{1.5}$$

The TFD model of WB in [35] is a highly simplified version of the MD theory [30]. The only cases where the TFD model of WB [35] produces exactly the same TFD relation as the MD theory [30] does are under constant normal force and satisfy either of the following conditions: (1) In the virgin loading case, i.e.,

$Q^* = 0$, and (2) in the unloading from the virgin loading after the maximum tangential force have reached very close to frictional limit, i.e., $|Q| \approx \mu P$. For all other cases, the TFD model of WB [35] does differ significantly from the MD theory [30] (see [15,32]). Thus, not only that the TFD model of WB in [35] is not accurate compared to the MD theory [30], but by addressing only *elastic* contact while ignoring plastic deformation, this TFD model of WB is *not* consistent with their NFD model [35], which accounts for plastic deformation at contact in a highly simplified manner (e.g., lack of accuracy and leading to a constant coefficient of restitution) [24].

1.3. A new elasto-plastic NFD model

The elasto-plastic NFD model presented in [2] accounts for both elastic and plastic deformations. A main feature of this elasto-plastic NFD model is an additive decomposition of the contact radius. In an elasto-plastic contact between two spheres subjected to a normal contact force P, the radius of the contact area is larger than the contact radius a^{e} determined by Hertz theory (for elastic contact), because of the plastic deformation. Let a^{ep} denote the contact radius for elasto-plastic contact, we have $a^{\mathrm{ep}} \geqslant a^{\mathrm{e}}$. We decompose the contact radius into the sum of an elastic part, denoted by a^{e} and determined by Hertz theory, and a plastic (correction) part (caused by plastic deformation) denoted by a^{p}, i.e.,

$$a^{\mathrm{ep}} = a^{\mathrm{e}} + a^{\mathrm{p}}. \tag{1.6}$$

It is noted that the above decomposition of the contact radius is parallel to the decomposition of total elasto-plastic strain ϵ^{ep} into elastic strain ϵ^{e} and plastic strain ϵ^{p} in the continuum theory of elasto-plasticity

$$\epsilon^{\mathrm{ep}} = \epsilon^{e} + \epsilon^{\mathrm{p}}. \tag{1.7}$$

Based on FEA results of normal contact between two elastic-perfectly-plastic spheres, we suggest the following model for the plastic correction contact radius a^{p}

$$a^{\mathrm{p}} = \begin{cases} C_a \langle P - P_Y \rangle (m) & \text{for loading,} \\ C_a \langle P_{\max} - P_Y \rangle (m) & \text{for unloading,} \end{cases} \tag{1.8}$$

where P_Y is the normal contact force when incipient yield occurs, C_a is a constant dependent on the radii of the spheres and on the material properties of the spheres, and the operator $\langle\rangle$ designates the MacCauley bracket defined by

$$\langle x \rangle = \begin{cases} 0 & \text{for } x \leqslant 0, \\ x & \text{for } x > 0. \end{cases} \tag{1.9}$$

The coefficient C_a can be evaluated based on either FEA results [31] or on simple experiments on granular materials [40].

With the elastic contact radius a^{e} determined from Hertz theory and with the plastic correction contact radius a^{p} determined from (1.8) above, the elasto-plastic contact radius a^{ep}, as obtained from (1.6) can be used to determine the normal displacement of the contact α by

$$2\alpha = \frac{(a^{\mathrm{ep}})^2}{R^*_{\mathrm{p}}} = \frac{(a^{\mathrm{e}} + a^{\mathrm{p}})^2}{C_{\mathrm{R}}(P) R^*}, \tag{1.10}$$

where $R^*_{\mathrm{p}} = C_{\mathrm{R}}(P) R^*$ is the radius of relative contact curvature after plastic deformation occurs, and is modified from the elastic radius R^* of contact curvature by a multiplicative factor $C_{\mathrm{R}}(P)$. Let ${}_{(i)}R$ and ${}_{(j)}R$ be the radii of the two spheres in contact, the radius R^* of contact curvature is defined as

$$R^* := \left(\frac{1}{{}_{(i)}R} + \frac{1}{{}_{(j)}R} \right)^{-1}. \tag{1.11}$$

The curvature modification coefficient $C_{\mathrm{R}}(P)$ is a function of the normal contact force P and of the mechanical properties of the two spheres in contact. For example, for two identical aluminum spheres (with radius $R = 0.1$ m) in contact as described in [2], the curvature modification coefficient $C_{\mathrm{R}}(P)$ is expressed as

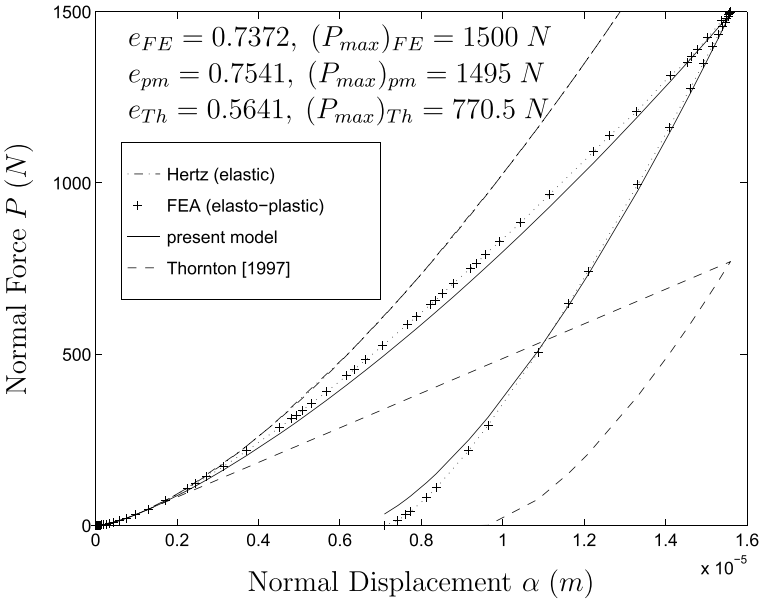

Fig. 2. Normal force P versus normal displacement α by different models from the FEA displacement path for the loading and unloading path with $P_{\max}$.

$$C_{\mathrm{R}}(P) = \begin{cases} 1.0 & \text{for } P \leqslant P_Y, \\ 1.0 + K_c\langle P - P_Y\rangle & \text{for } P > P_Y, \end{cases} \tag{1.12}$$

where $K_c = 2.69 \times 10^{-4}\ \mathrm{N}^{-1}$ is a constant. We refer the readers to [2,31] for more details on the elasto-plastic NFD model and finite element analyses of elasto-plastic contact problems.

It is shown in [2] that the above elasto-plastic NFD model accurately captures the effects of plastic deformation in the NFD relationship (as shown in Fig. 2).

In the following, we present an elasto-plastic TFD model that is completely consistent with the above elasto-plastic NFD model for use in DEM simulations of granular flows. It is believed that the present set of elasto-plastic-frictional NFD and TFD models is the first of its kind, i.e., a set of consistent models in the normal and tangential directions for elasto-plastic-frictional contact.

As pointed out in [2], the elasto-plastic NFD model is general in accounting for plastic deformation by the additive decomposition of contact radius (1.6) and the modification of contact curvature (in (1.10)), but the value of some of the model parameters (e.g., C_a and K_c) dependent on the material properties and the geometry of the spheres in contact. Similarly, the elasto-plastic TFD model presented in this paper is a general approach, and the same set of model parameters, including C_a and K_c, are employed to account for the effect of plastic deformation.

2. The elastic tangential force–displacement (TFD) model

We review in this section the TFD model for *elastic* frictional contact proposed in [32]. This TFD model serves as the foundation for the new TFD model for *elasto-plastic* frictional contact to be presented in the subsequent section.

2.1. TFD relationship under constant normal force

The TFD model of WB [35] only agrees with the MD theory [30] in the simplest case where the normal force P is constant. When both the normal force P and the tangential force Q vary, as occurred frequently in the collisions in granular flows, the TFD model of WB [35] introduces large errors in the δ–Q (FD) relationship, i.e., the relationship between the tangential displacement δ and the tangential force Q. We propose in [32] an

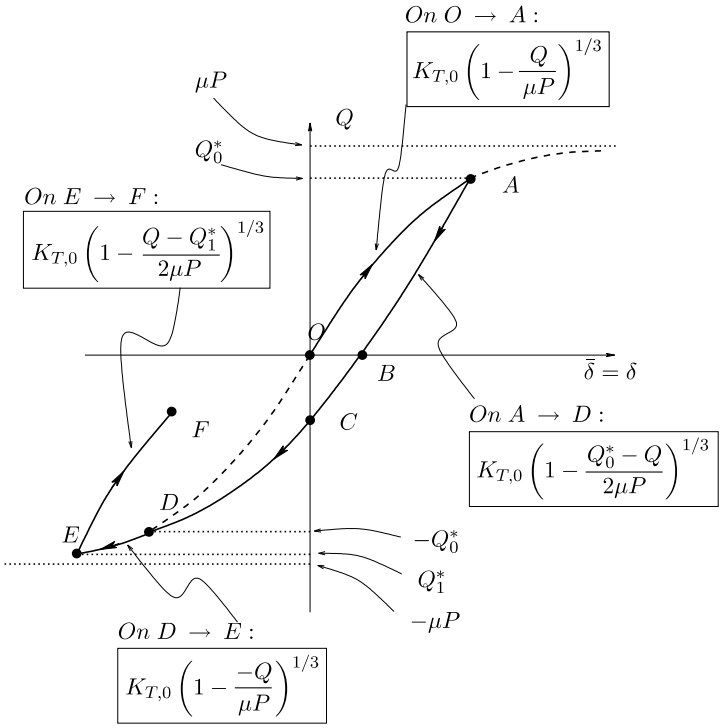

Fig. 3. Tangential stiffness K_T for constant normal force P.

accurate and efficient TFD model that correctly accounts for the case where both P and Q are varying in elastic frictional contact. This improved TFD model is shown to produce DEM simulation results that corroborate with experimental results, whereas other TFD models did not [32].

The TFD model in [32] is an incremental model that determines the tangential contact force Q_{n+1} at the new time step $(n+1)$ based on the given incremental tangential displacement $\Delta\delta_{n+1}$ and previously calculated force and displacement histories. For the loading cases with a constant normal contact force P, the TFD model in [32] follows exactly the MD theory [30] (Fig. 3).

The incremental formula for computing the tangential force is the same as (1.3), which was used in the TFD model of WB [35], but the tangential stiffness is determined in a different manner by

$$K_{\mathrm{T}} = \begin{cases} K_{\mathrm{T},0}\left(1-\dfrac{Q-Q^*}{2\mu P}\right)^{1/3} & \text{for } Q \text{ increasing } (\nearrow) \text{ and } |Q| < |Q^*|, \\ K_{\mathrm{T},0}\left(1-\dfrac{Q}{\mu P}\right)^{1/3} & \text{for } Q \text{ increasing } (\nearrow) \text{ and } |Q| \geqslant |Q^*|, \\ K_{\mathrm{T},0}\left(1-\dfrac{Q^*-Q}{2\mu P}\right)^{1/3} & \text{for } Q \text{ decreasing } (\searrow) \text{ and } |Q| < |Q^*|, \\ K_{\mathrm{T},0}\left(1+\dfrac{Q}{\mu P}\right)^{1/3} & \text{for } Q \text{ decreasing } (\searrow) \text{ and } |Q| \geqslant |Q^*|, \end{cases} \tag{2.1}$$

where $K_{\mathrm{T},0}$ is the tangential stiffness for initial loading. According to the MD theory [30], the tangential stiffness $K_{\mathrm{T},0}$ is determined by

$$K_{\mathrm{T},0} = 8a\left(\frac{2-{}_{(i)}\nu}{{}_{(i)}G}+\frac{2-{}_{(j)}\nu}{{}_{(j)}G}\right)^{-1}, \tag{2.2}$$

where a is the contact radius for a given normal force P, as determined by (3.1) (i.e., Hertz theory), ${}_{(i)}\nu$ and ${}_{(j)}\nu$ the Poisson's ratios of spheres (i) and (j), respectively, and ${}_{(i)}G$ and ${}_{(j)}G$ the shear moduli of the spheres (i) and (j) in contact, respectively.

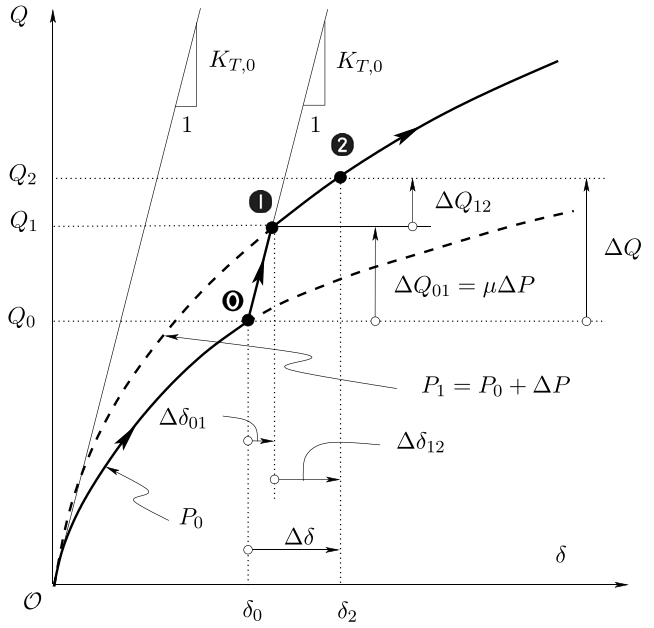

Fig. 4. TFD relationship for P increasing, Q increasing.

2.2. TFD relationship under varying normal force

In the following, we briefly review how the change of the normal contact force P is accounted for in the loading cases where both P and Q are varying. We consider four cases, out of eleven cases considered in [30]. More detailed discussion can be found in [32].

2.2.1. Case of P increasing, Q increasing

Let ΔP and ΔQ be the increments of normal force and tangential force, respectively. Let state ⓪ be the state of the FD relationship at the previous time step, with the normal force, the tangential force, and the tangential displacement denoted by $\{P_0, Q_0, \delta_0\}$, respectively (see Fig. 4). Assuming that the loading up to state ⓪ had been a *simple* loading (e.g. [30]), we first increase the normal force to $P_1 = P_0 + \Delta P$, then increase the tangential force by ΔQ; there are two subcases: $\Delta Q \geqslant \mu\Delta P$ and $\Delta Q < \mu\Delta P$.

For the subcase where $\Delta Q \geqslant \mu\Delta P$, the tangential force increment ΔQ is decomposed into two parts: ΔQ_{01} and ΔQ_{12} such that $\Delta Q = \Delta Q_{01} + \Delta Q_{12}$ with $\Delta Q_{01} = \mu\Delta P$. According to the MD theory [30], when both ΔP and ΔQ are very small ($\Delta P \to 0$, $\Delta Q \to 0$), the tangential stiffness for the first part of the increment, i.e., ΔQ_{01} is the same as the initial tangential stiffness for P constant loading case, i.e.,

$$(K_{\mathrm{T}})_{01} = (K_{\mathrm{T},0})_{P=P_0}. \tag{2.3}$$

State ❶, after being reached at the end of the first part ΔQ_{01}, is equivalent to a state of initial loading under the constant normal force $P = P_1 = P_0 + \Delta P$. In this situation, the tangential stiffness for the second part of ΔQ_{12} takes the same expression as in (2.1) for the case under constant normal force P, i.e.,

$$(K_{\mathrm{T}})_{12} = (K_{\mathrm{T},0})_{P=P_1}\left(1 - \frac{Q_1}{\mu P_1}\right)^{1/3}, \tag{2.4}$$

where $Q_1 = Q_0 + \Delta Q_{01} = Q_0 + \mu\Delta P$ as shown in Fig. 4.

The coefficient $(K_{\mathrm{T},0})_{P=P_1}$ is the initial tangential stiffness for the TFD curve under constant normal loading $P = P_1$, determined by (2.2). Therefore, at state ❷

$$Q_2 = Q_0 + \mu\Delta P + (K_{\mathrm{T}})_{12}\Delta\delta_{12} = Q_0 + \mu\Delta P + (K_{\mathrm{T}})_{12}\left(\Delta\delta - \frac{\mu\Delta P}{(K_{\mathrm{T},0})_{P=P_0}}\right), \tag{2.5}$$

and

$$\delta_2 = \delta_0 + \frac{\mu\Delta P}{(K_{\mathrm{T},0})_{P=P_0}} + \frac{\Delta Q - \mu\Delta P}{(K_{\mathrm{T}})_{12}}. \tag{2.6}$$

For the subcase where $\Delta Q < \mu\Delta P$, the tangential force increment is not large enough to complete the transition from state ⓪ to state ❶ shown in Fig. 4. We use the following FD relationship for this case

$$Q' = Q_0 + (K_{\mathrm{T},0})_{P=P_0}\Delta\delta, \tag{2.7}$$

where $\Delta\delta < \Delta\delta_{01} = \dfrac{\mu\Delta P}{(K_{\mathrm{T},0})_{P=P_0}}$. Since this state is not a state equivalent to the case of tangential loading under constant normal force P, the loading history after this step of loading increment is no longer a *simple loading* history.

In DEM simulations, the tangential force Q_{n+1} is determined from the computed displacement δ_{n+1} at time t_{n+1}. The state of the system (forces and displacements) at time t_n is thought to be at state ⓪, as shown in Fig. 4. Let $\Delta\delta = \delta_{n+1} - \delta_n$, and $\Delta P = P_{n+1} - P_n$. When $\Delta\delta \geqslant \dfrac{\mu\Delta P}{(K_{\mathrm{T},0})_{P=P_n}}$, we have

$$Q_{n+1} = Q_n + \mu\Delta P + K_{\mathrm{T},n}\left(\Delta\delta - \frac{\mu\Delta P}{(K_{\mathrm{T},0})_{P=P_n}}\right) \tag{2.8}$$

where the current tangential stiffness $K_{\mathrm{T},n}$ is determined by (2.1) to yield

$$K_{\mathrm{T},n} = (K_{\mathrm{T},0})_{P=P_{n+1}}\left(1 - \frac{Q_n + \mu\Delta P}{\mu P_{n+1}}\right)^{1/3}. \tag{2.9}$$

When $\Delta\delta < \dfrac{\mu\Delta P}{(K_{\mathrm{T},0})_{P=P_n}}$, the tangential force Q_{n+1} is determined by

$$Q_{n+1} = Q_n + (K_{\mathrm{T},0})_{P=P_n}\Delta\delta. \tag{2.10}$$

2.2.2. Case of P decreasing, Q increasing

Let $\Delta P = P_{n+1} - P_n$ and $\Delta\delta = \delta_{n+1} - \delta_n$. Clearly, $\Delta P < 0$ and $\Delta\delta > 0$ for this loading case. According to the TFD model [32], the tangential force Q_{n+1} at time t_{n+1} can be expressed by

$$Q_{n+1} = Q_n + K_{\mathrm{T},n}\left(\Delta\delta - \frac{\mu\Delta P}{(K_{\mathrm{T},0})_{P=P_n}} + \frac{\mu\Delta P}{K'_{\mathrm{T},n}}\right), \tag{2.11}$$

where $K_{\mathrm{T},n}$ is the current tangential stiffness, $K'_{\mathrm{T},n}$ an intermediate tangential stiffness for this loading step. The stiffness coefficients $K_{\mathrm{T},n}$ and $K'_{\mathrm{T},n}$ are determined by

$$K_{\mathrm{T},n} = (K_{\mathrm{T},0})_{P=P_{n+1}}\left(1 - \frac{Q_n}{\mu P_{n+1}}\right)^{1/3}, \tag{2.12}$$

and

$$K'_{\mathrm{T},n} = (K_{\mathrm{T},0})_{P=P_{n+1}}\left(1 - \frac{Q_n + \mu\Delta P}{\mu P_{n+1}}\right)^{1/3}. \tag{2.13}$$

2.2.3. Case of P increasing, Q decreasing

Again, with $\Delta P = P_{n+1} - P_n$ and $\Delta\delta = \delta_{n+1} - \delta_n$, we have $\Delta P > 0$ and $\Delta\delta < 0$ for this loading case. There are two subcases that need to be considered: $|\Delta\delta| \geqslant \dfrac{\mu\Delta P}{(K_{\mathrm{T},0})_{P=P_n}}$ and $|\Delta\delta| < \dfrac{\mu\Delta P}{(K_{\mathrm{T},0})_{P=P_n}}$.

For the first subcase where when $|\Delta\delta| \geqslant \dfrac{\mu\Delta P}{(K_{\mathrm{T},0})_{P=P_n}}$, according to the TFD model in [32], the tangential force can be expressed as

$$Q_{n+1} = Q_n - \mu\Delta P + K_{\mathrm{T},n}\left(\Delta\delta + \frac{\mu\Delta P}{(K_{\mathrm{T},0})_{P=P_n}}\right), \tag{2.14}$$

where $K_{\mathrm{T},n}$ is the tangential stiffness determined by

$$K_{\mathrm{T},,n} = (K_{\mathrm{T},0})_{P=P_{n+1}}\left(1 - \frac{Q_n^* + \mu\Delta P - (Q_n - \mu\Delta P)}{2\mu P_{n+1}}\right)^{1/3}. \tag{2.15}$$

After this step, the tangential force for the last turning point is updated using $Q_{n+1}^* = Q_n^* + \mu\Delta P$.

For the subcase where $|\Delta\delta| < \dfrac{\mu\Delta P}{(K_{\mathrm{T},0})_{P=P_n}}$, the tangential force is then computed by

$$Q_{n+1} = Q_n + (K_{\mathrm{T},0})_{P=P_n}\Delta\delta. \tag{2.16}$$

After this step of loading increment, the loading history is no longer a *simple loading* history.

2.2.4. Case of P decreasing, Q decreasing

With $\Delta P = P_{n+1} - P_n$ and $\Delta\delta = \delta_{n+1} - \delta_n$, we now encounter three subcases in this loading case: (i) $Q_n \leqslant Q_n^* + 2\mu\Delta P$, and for $Q_n > Q_n^* + 2\mu\Delta P$, there are two additional subcases: (ii) $Q_n^* + 2\mu\Delta P < Q_n < Q_n^* + \mu\Delta P$, and (iii) $Q_n^* + \mu\Delta P \leqslant Q_n$.

In the first subcase where $Q_n \leqslant Q_n^* + 2\mu\Delta P$, the tangential force can be expressed as

$$Q_{n+1} = Q_n + K_{\mathrm{T},n}\left(\Delta\delta + \frac{\mu\Delta P}{(K_{\mathrm{T},0})_{P=P_n}} - \frac{\mu\Delta P}{K'_{\mathrm{T},n}}\right), \tag{2.17}$$

where the stiffness coefficients $K_{\mathrm{T},n}$ and $K'_{\mathrm{T},n}$ are determined by

$$K_{\mathrm{T},n} = (K_{\mathrm{T},0})_{P=P_{n+1}}\left(1 - \frac{Q_{n+1}^* - Q_n}{2\mu P_{n+1}}\right)^{1/3}, \tag{2.18}$$

and

$$K'_{\mathrm{T},n} = (K_{\mathrm{T},0})_{P=P_{n+1}}\left(1 - \frac{Q_{n+1}^* - (Q_n - \mu\Delta P)}{2\mu P_1}\right)^{1/3}, \tag{2.19}$$

with $Q_{n+1}^* = Q_n^* + \mu\Delta P$ being the updated (equivalent) tangential force at the last turning point.

For the subcase where $Q_n > Q_n^* + 2\mu\Delta P$, and $Q_n^* + 2\mu\Delta P < Q_n < Q_n^* + \mu\Delta P$, the tangential force Q_{n+1} is computed by

$$Q_{n+1} = Q_n^* + \mu\Delta P + K_{\mathrm{T},n}\left(\Delta\delta - \frac{Q_n^* + \mu\Delta P - Q_n}{(K_{\mathrm{T},0})_{P=P_n}}\right), \tag{2.20}$$

where the tangential stiffness $K_{\mathrm{T},n+1}$ is determined by

$$K_{\mathrm{T},n} = (K_{\mathrm{T},0})_{P=P_{n+1}}\left(1 - \frac{Q_n^* + \mu\Delta P - Q_n}{2\mu P_{n+1}}\right)^{1/3}. \tag{2.21}$$

For the subcase where $Q_n > Q_n^* + 2\mu\Delta P$, and $Q_n^* + \mu\Delta P \leqslant Q_n$, there are subsubcases to consider. If $|\Delta\delta| \leqslant |\dfrac{Q_n^* + \mu\Delta P - Q_n}{K'_{\mathrm{T},n}}|$, the tangential force is computed by

$$Q_{n+1} = Q_n^* + \mu\Delta P + K_{\mathrm{T},n}\left(\Delta\delta - \frac{Q_n^* + \mu\Delta P - Q_n}{K'_{\mathrm{T},n}}\right), \tag{2.22}$$

where the tangential stiffness $K'_{\mathrm{T},n}$ is determined by

$$K'_{\mathrm{T},n} = (K_{\mathrm{T},0})_{P=P_n}\left(1 - \frac{Q_n^* - Q_n - \mu\Delta P}{4\mu P_n}\right)^{1/3}. \tag{2.23}$$

For the stiffness coefficient $K_{\mathrm{T},n}$, if $|\Delta\delta| \leqslant |\frac{Q_n^* + \mu\Delta P - Q_n}{K'_{\mathrm{T},n}}|$, where $K'_{\mathrm{T},n}$ is computed by (2.23), then

$$K_{\mathrm{T},n} = (K_{\mathrm{T},0})_{P=P_{n+1}} \left(1 - \frac{Q_n^* + \mu\Delta P}{\mu P_{n+1}}\right)^{1/3}, \tag{2.24}$$

else if $|\Delta\delta| > |\frac{Q_n^* + \mu\Delta P - Q_n}{K'_{\mathrm{T},n}}|$, where $K'_{\mathrm{T},n}$ is computed by (2.23), then

$$K_{\mathrm{T},n} = (K_{\mathrm{T},0})_{P=P_{n+1}}. \tag{2.25}$$

We refer the readers to [30,32] for detailed derivation of the above formulae.

3. The elasto-plastic frictional TFD model

The elasto-plastic frictional TFD model proposed in this paper is consistent with the elasto-plastic NFD model presented in [2]. It is developed from the TFD model in [32] for elastic-frictional contact summarized in Sections 2.1 and 2.2. The account for the effect of plastic deformation is based on the same formalism used for the elasto-plastic NFD model, i.e., the additive decomposition of the elasto-plastic contact radius a^{ep} by (1.6), and the modification of the radius R^* of local contact curvature by (1.10). In the following, we will discuss formulation of the TFD model that accounts for plastic deformation, and present the pseudo code for the proposed TFD model.

3.1. The effect of plastic deformation

In the elasto-plastic NFD model in [2], to account for the effect of plastic deformation on the normal force–displacement relationship, we introduce the additive decomposition of elasto-plastic contact radius a^{ep} into the elastic part a^{e} and the plastic part a^{p}, according to (1.6). Following Hertz theory, the elastic contact radius a^{e} is determined by

$$a^{\mathrm{e}} = \left(\frac{3PR^*}{4E^*}\right)^{1/3}, \tag{3.1}$$

where R^* is the equivalent radius of relative contact curvature defined by

$$R^* := \left(\frac{1}{{}_{(i)}R} + \frac{1}{{}_{(j)}R}\right)^{-1}, \tag{3.2}$$

E^* the equivalent elastic modulus for the contact defined by

$$E^* := \left(\frac{1 - {}_{(i)}\nu^2}{{}_{(i)}E} + \frac{1 - {}_{(j)}\nu^2}{{}_{(j)}E}\right)^{-1}. \tag{3.3}$$

In addition to the increase in the contact area, another feature of elasto-plastic contact is that the irreversible plastic deformation tends to flatten the contact surface, thus decreases the relative contact curvature. Fig. 5 shows the increase of the radius of contact curvature, as caused by plastic deformation when a sphere contacts a rigid planar surface. In [2], we use a coefficient $C_{\mathrm{R}}(P) \geqslant 1.0$ to modify the local radius of contact curvature. For given material properties the radii of spheres in contact, the coefficient $C_{\mathrm{R}}(P)$ is determined by the normal force P (using e.g. (1.12)).

In 3-D finite element analyses (FEA) of two identical elastic-perfectly-plastic spheres contacting against each other with friction [31], we observe the following force–displacement (FD) behavior of the tangential contact stiffness:

1. When the contact is in the elastic range, i.e., without yield and plastic deformation, the FD behavior in normal direction follows the Hertz theory; the FD behavior in tangential direction follows the MD theory [30].
2. For aluminum, which is the material employed in the FEA in [31], while the plastic zone under the combined loading of P and Q remains very close to the plastic zone created by the normal force P alone, plastic deformation clearly affects the TFD behavior (see Remark 3.1 for more explanation).

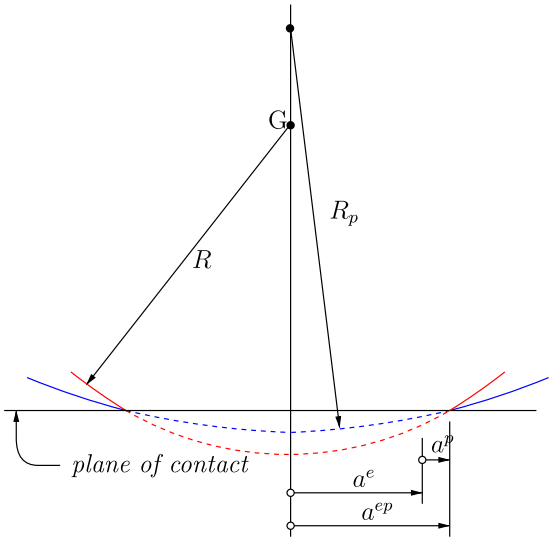

Fig. 5. Sphere in contact with a rigid planar surface: plastic deformation increases the radius of local relative contact curvature from R to R_p.

3. In the case where the normal force P is applied on the sphere until its magnitude becomes very large compared to the yield normal force P_Y ($P \gg P_Y$), and then held constant while the tangential force Q is applied with increasing magnitude, even though there is a large amount of plastic deformation involved, the TFD behavior is stiffer than that obtained for the elastic case using the MD theory [30] (see Remark 3.1 for more explanation, and also [2]). Fig. 6 shows the TFD curves, computed by FEA and by the MD theory [30], for two identical aluminum spheres of radius $R = 0.1$ m in contact with each other. The spheres are subjected to a constant normal load $P = 2600$ N and varying tangential force Q. FEA results were obtained for elasto-plastic behavior of the material.

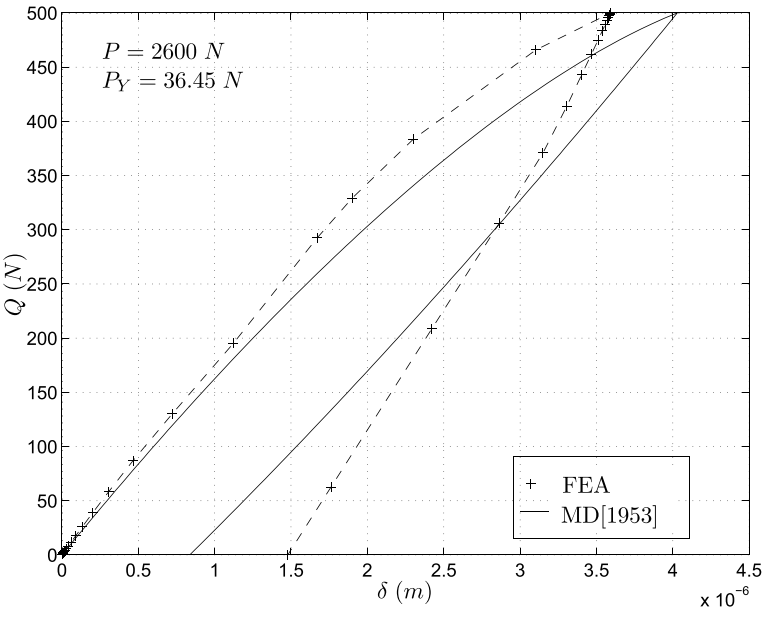

Fig. 6. Two identical aluminum spheres in contact: TFD curves from FEA of elasto-plastic sphere material, and from Mindlin & Deresiewicz [1953] (MD[1953]) elastic theory. Constant normal force $P = 2600$ N, and varying tangential force Q.

4. When both the normal force P and the tangential force Q are increasing, the FD behavior in the normal direction follows what described in [2], i.e., softer than Hertz (elastic) theory; the FD behavior in the tangential direction is also softer than that from the MD (elastic) theory [30], as a result of the plastic deformation.
5. The TFD curves for both elastic and elasto-plastic materials display a hysteresis effect when the applied tangential force Q goes through cycles of loading, unloading and reloading. The TFD curve for the elasto-plastic material display a softer behavior during loading. Fig. 7 shows the FEA results of the same sphere as in Fig. 6, subjected to varying normal and tangential forces (P and Q), and a comparison with the MD elastic-frictional contact theory [30]. The step like behavior in the TFD curve during loading is due to the change in the normal load P throughout the loading phase. The maximum magnitude of P is $P_{\max} = 1500$ N.

Remark 3.1. Since $Q \leqslant \mu P$ throughout the loading and unloading stages, and since the coefficient of friction chosen was $\mu = 0.2$, the effect of the tangential force Q on the plastic deformation is relatively smaller than that of the normal force P.

Also, it is interesting to observe that plastic deformation makes the TFD curve stiffer, compared to that of elastic material, in the case where the normal load P is constant. The reason is that when the sphere yields under the normal force P that is much larger than the yield normal force P_Y, the contact area is also much larger than that of the elastic case. It follows that there is more contact area to resist the tangential force Q through friction. On the other hand, when both P and Q are varying, plastic deformation affects the TFD relationship that is softer and has a step-like pattern shown in Fig. 7. We refer the readers to [31] for more details.

Based on the FEA results, it can be concluded that the plastic deformation affects the TFD behavior in following ways: (i) Increase the contact radius a, and thus increase the tangential stiffness. (ii) Increase the radius of local contact curvature R^*_{p}, and thus increase the tangential stiffness. (iii) The plastic zone weakens

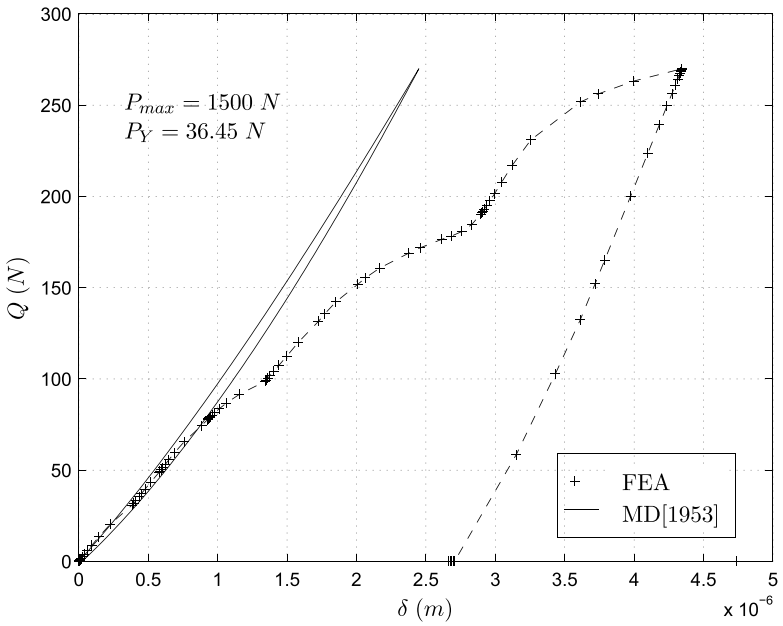

Fig. 7. Two identical aluminum spheres in contact: TFD curves from FEA of elasto-plastic sphere material, and from Mindlin & Deresiewicz [1953] (MD[1953]) elastic theory. Varying normal force P and tangential force Q.

the resistance to the tangential force, and thus decreases the tangential stiffness. For most of the loading cases considered, FEA yields a TFD relationship that is softer than that of the MD theory [30] for elastic frictional contact.

Let us look at the TFD relationship described in Sections 2.1 and 2.2. Only the calculation of initial tangential stiffness $K_{T,0}$ (see (2.2)) is connected to the effect of plastic deformation described above. Considering that the TFD curves from elasto-plastic FEA results retain the same shape as those from the MD theory [30], we retain much of the formulation described in Sections 2.1 and 2.2 to account for the effect of changing in the normal force, and this for all loading cases. Recall that

$$K_{T,0} = 8a\left(\frac{2-{}_{(i)}\nu}{{}_{(i)}G}+\frac{2-{}_{(j)}\nu}{{}_{(j)}G}\right)^{-1}, \tag{2.2}$$

If one inserts the increased elasto-plastic contact radius a^{ep} into (2.2), the tangential stiffness is increased to account for the effect of plastic deformation. In this case, the weakening of tangential stiffness by plastic deformation could not be properly represented. For this reason, we introduce the equivalent Young's modulus $(E^*)^{ep}$ for the elasto-plastic contact in the tangential direction.

For the cases where the normal force P is increasing, we replace a by a^{ep}, R^* by R^*_p, and E by $(E^*)^{ep}$, in (3.1) to obtain

$$a^{ep} = \left(\frac{3PR^*_p}{4(E^*)^{ep}}\right)^{1/3}. \tag{3.4}$$

Therefore, for P increasing,

$$(E^*)^{ep} = \frac{3PR^*_p}{4(a^{ep})^3} = \frac{3PC_R(P)R^*}{4(a^{ep})^3}. \tag{3.5}$$

From (3.5) it can be seen that since the contact radius $a^{ep} > a^e$ when there is a plastic deformation, this enlarged contact area tends to decrease $(E^*)^{ep}$, if the other quantities are held constant. On the other hand, since the radius of contact curvature $R^*_p \geqslant R^*$ when there is plastic deformation, this increase in the radius of contact curvature tends to increase $(E^*)^{ep}$. For most cases, the effect of a^{ep} is stronger, and thus the equivalent elasto-plastic Young's modulus $(E^*)^{ep}$ is usually less than the original material Young's modulus E, as if the Young's modulus is weakened by the plastic deformation. It should be noticed that since $(E^*)^{ep}$ is proportional to $R^*_p = C_R(P)R^*$ as given in (3.5), the use of $(E^*)^{ep}$ in the computation of the tangential stiffness in the TFD relationship therefore also accounts for the effect of the increase in the radius of contact curvature due to plastic deformation.

Recalling that $G = \dfrac{E}{2(1+\nu)}$, and assuming that the two spheres in contact have the same Poisson's ratios, i.e., ${}_{(i)}\nu = {}_{(j)}\nu = \nu$, we can rewrite (2.2) as follows:

$$K_{T,0} = 4a^{ep}\left(\frac{(1+\nu)(2-\nu)}{{}_{(i)}E}+\frac{(1+\nu)(2-\nu)}{{}_{(j)}E}\right)^{-1}. \tag{3.6}$$

We can express the initial tangential stiffness for the TFD relationship in terms of the Young's modulus E^* by using (3.3) in (3.6). Once this step is done, we again replace E^* by $(E^*)^{ep}$ to account for plastic deformation in the computation of $K_{T,0}$ and obtain

$$K_{T,0} = 4a^{ep}(E^*)^{ep}\left(\frac{1-\nu}{2-\nu}\right). \tag{3.7}$$

Therefore, when the normal force P is increasing, expression (3.7) is used in the computation of the tangential stiffness in the TFD relationship to account for the effect of plastic deformation.

When the normal force P is decreasing, the plastic deformation is frozen, as the spheres undergo elastic unloading. Therefore, the following formula is used to modify the equivalent elastic modulus

$$(E^*)^{ep} = \frac{3PC_R(P_{max})R^*}{4(a^e)^3}, \tag{3.8}$$

where the value of C_R is frozen at is value at $P = P_{max}$, and the contact radius in the denominator is the elastic part a^e. The tangential stiffness in the TFD relationship is computed using expression (3.7) for the initial tangential stiffness $K_{T,0}$, but with $(E^*)^{ep}$ computed from (3.8).

It should be noticed that since plastic deformation is mainly attributed to the normal force P, when P remains a constant during the loading or unloading of the tangential force Q, the plastic zone is considered as unchanged. Therefore, the modification of tangential stiffness for the case where P is a constant should be similar to that of the case where P is decreasing, i.e., (3.8) is used to compute the equivalent Young's modulus $(E^*)^{ep}$.

The modification of the tangential stiffness of the TFD relationship can properly account for the effect of plastic deformation for a range of the ratio of increment of P over increment in Q. Further work is needed to extend this range, which is large enough for granular flow simulations. We refer the readers to [1] for more detailed discussion.

Now we can see that the approach to account for the effect of plastic deformation on TFD relationship involves both the additive decomposition of the contact radius a^{ep} (in the computation of $K_{T,0}$ by (3.7)) and the modification of contact curvature (as in the equivalent elastic modulus by (3.5)). Therefore, the present elasto-plastic TFD model is consistent with the elasto-plastic NFD model in [2]. Again, the TFD model presented here is general, and the *values* of some model parameters (e.g., C_a and K_c) of course depend on the material and the geometry of the spheres in contact. This is similar to the construction of plasticity model in continuum mechanics as we described in [2].

3.2. Algorithm and implementation of the new elasto-plastic TFD model

In a DEM simulation code, the increment of tangential displacement between two spheres in contact is evaluated by the relative position and velocities of these two spheres in each timestep of numerical integration (see [15]). At time t_{n+1}, the normal contact force P_{n+1} is computed by the elasto-plastic NFD model that is consistent with the present TFD model, and whose algorithm is presented in [2]. We use this present elasto-plastic TFD model to compute the current tangential contact force Q_{n+1} based on the increment of tangential displacement $\Delta\delta_{n+1} = \delta_{n+1} - \delta_n$, and on the loading history previously calculated.

We can see, from previous discussion, that the effect of plastic deformation on the TFD relationship is accounted for by using (3.7) to compute the initial tangential stiffness using the elasto-plastic contact radius a^{ep} and the equivalent Young's modulus $(E^*)^{ep}$. Noticing that the shape of the TFD curves obtained from elasto-plastic FEA is similar to that obtained from the MD theory [30] and from the TFD model in [32], we employ the same procedure as described in Section 2.2 to account for the effect of varying normal force P. The implementation of the present elasto-plastic TFD model is described algorithmically in the pseudo code below. In Algorithm 3.1, the elasto-plastic NFD model is the one presented in [2]. Therefore, the implementation of the proposed elasto-plastic TFD model follows Algorithm 3.1.

Algorithm 3.1. Elasto-plastic TFD model: displacement-driven version.

Input: ${}_{(i)}R, {}_{(j)}R, E, \nu, \sigma_Y$.
P_Y calculated using the elasto-plastic NFD model.
P_n, P_{n+1}, and P_{max} calculated using the elasto-plastic NFD model.
a^e_{n+1}, a^p_{n+1}, and a^{ep}_{n+1} calculated using the elasto-plastic NFD model.
Displacement $\{\delta_n, \delta_{n+1}\}$, forces $\{Q_n, Q^*_n\}$.
Goal: compute next tangential force Q_{n+1}.
Initialization: $Q^*_0 = 0$, $Q_{inc} =$ **true**.
Calculate $\Delta P_{n+1} = P_{n+1} - P_n$.
Calculate $\Delta\delta_{n+1} = \delta_{n+1} - \delta_n$.
Set $Q^*_{n+1} = Q^*_n$.
①**if** $\Delta P_{n+1} = 0$ (P constant)

②**if** $P_{n+1} \leqslant P_Y$ (elastic case)
  Calculate $K_{\mathrm{T},0}$ via (2.2).
②**elseif** $P_{n+1} > P_Y$ (plastic case)
    Calculate $(E^*)^{\mathrm{ep}}$ via (3.8).
    Calculate $K_{\mathrm{T},0}$ via (3.7).
  ②**endif**
③**if** $\Delta\delta_{n+1} \geqslant 0$ (Q increasing)
  Calculate $K_{\mathrm{T},n}$ via (2.1).
  Calculate Q_{n+1} via (1.3).
  Set $Q_{\mathrm{inc}} =$ **true**.
③**elseif** $\Delta\delta_{n+1} < 0$ (Q decreasing)
    if $Q_{\mathrm{inc}} =$ **true**
      Set $Q^*_{n+1} = Q_n$.
    endif
    Calculate $K_{\mathrm{T},n}$ via (2.1).
    Calculate Q_{n+1} via (1.3).
    Set $Q_{\mathrm{inc}} =$ **false**.
③**endif**
①**elseif** $\Delta P_{n+1} > 0$ (P increasing)
  ④**if** $P_{n+1} \leqslant P_Y$ (elastic case)
    Calculate $K_{\mathrm{T},0}$ via (2.2).
  ④**elseif** $P_{n+1} > P_Y$ (plastic case)
      Calculate $(E^*)^{\mathrm{ep}}$ via (3.5).
      Calculate $K_{\mathrm{T},0}$ via (3.7).
  ④**endif**
  ⑤**if** $\Delta\delta_{n+1} \geqslant 0$ (Q increasing)
    ⑥**if** $\Delta\delta_{n+1} \geqslant \dfrac{\mu\Delta P}{(K_{\mathrm{T},0})_{P=P_n}}$
      Calculate $K_{\mathrm{T},n}$ via (2.9).
      Calculate Q_{n+1} via. (2.8).
    ⑥**elseif** $\Delta\delta_{n+1} < \dfrac{\mu\Delta P}{(K_{\mathrm{T},0})_{P=P_n}}$
        Calculate Q_{n+1} via (2.10).
        WARNING: NOT a simple loading step.
    ⑥**endif**
    Set $Q_{\mathrm{inc}} =$ **true**.
  ⑤**elseif** $\Delta\delta_{n+1} < 0$ (Q decreasing)
    if $Q_{\mathrm{inc}} =$ **true**
      Set $Q^*_{n+1} = Q_n$.
    endif
    ⑦**if** $\|\Delta\delta_{n+1}\| \geqslant \dfrac{\mu\Delta P}{(K_{\mathrm{T},0})_{P=P_n}}$
      Calculate $K_{\mathrm{T},n}$ via (2.15).
      Calculate Q_{n+1} via (2.14).
    ⑦**elseif** $\|\Delta\delta_{n+1}\| < \dfrac{\mu\Delta P}{(K_{\mathrm{T},0})_{P=P_n}}$
        Calculate Q_{n+1} via (2.16).
        WARNING: NOT a simple loading step.
    ⑦**endif**
    Update $Q^*_{n+1} = Q^*_n + \mu\Delta P$.
    Set $Q_{\mathrm{inc}} =$ **false**.
  ⑤**endif**

①**elseif** $\Delta P_{n+1} < 0$ (P decreasing)
  ⑧**if** $P_{n+1} \leqslant P_Y$ (elastic case)
    Calculate $K_{\mathrm{T},0}$ via (2.2).
  ⑧**elseif** $P_{n+1} > P_Y$ (plastic case)
      Calculate $(E^*)^{\mathrm{ep}}$ via (3.8).
      Calculate $K_{\mathrm{T},0}$ via (3.7).
  ⑧**endif**
  ⑨**if** $\Delta\delta_{n+1} \geqslant 0$ (Q increasing)
    Calculate $K_{\mathrm{T},n}$ via (2.12).
    Calculate $K'_{\mathrm{T},n}$ via (2.13).
    Calculate Q_{n+1} via (2.11).
    Set $Q_{\mathrm{inc}} =$ **true**.
  ⑨**elseif** $\Delta\delta_{n+1} < 0$ (Q decreasing)
      if $Q_{\mathrm{inc}} =$ **true**
        Set $Q^*_{n+1} = Q_n$.
      endif
      ⑩**if** $Q_n \leqslant Q^*_{n+1} + 2\mu\Delta P$
        Calculate $K_{\mathrm{T},n}$ via (2.18).
        Calculate $K'_{\mathrm{T},n}$ via (2.19).
        Calculate Q_{n+1} via (2.17).
        Update $Q^*_{n+1} = Q^*_n + \mu\Delta P$.
      ⑩**elseif** $Q_n > Q^*_{n+1} + 2\mu\Delta P$
        ⑪**if** $Q^*_{n+1} + 2\mu\Delta P < Q_n < Q^*_{n+1} + \mu\Delta P$
          Calculate $K_{\mathrm{T},n}$ via (2.21).
          Calculate Q_{n+1} via (2.20).
          Update $Q^*_{n+1} = Q^*_n + \mu\Delta P$.
        ⑪**elseif** $Q^*_{n+1} + \mu\Delta P \leqslant Q_n$
            Calculate $K'_{\mathrm{T},n}$ via (2.23).
            ⑫**if** $\|\Delta\delta\| \leqslant \|\dfrac{Q^*_{n+1} + \mu\Delta P - Q_n}{K'_{\mathrm{T},n}}\|$
              Calculate $K_{\mathrm{T},n}$ via (2.24).
            ⑫**elseif** $\|\Delta\delta\| \leqslant \|\dfrac{Q^*_{n+1} + \mu\Delta P - Q_n}{K'_{\mathrm{T},n}}\|$
              Calculate $K_{\mathrm{T},n}$ via (2.25).
            ⑫**endif**
            Calculate Q_{n+1} via (2.22).
            Update $Q^*_{n+1} = Q^*_n + \mu\Delta P$.
        ⑪**endif**
      ⑩**endif**
    Set $Q_{\mathrm{inc}} =$ **false**.
  ⑨**endif**
①**endif**

4. Numerical examples: comparison with FEA results

We implemented the present elasto-plastic TFD model into a MATLAB code. The TFD curves produced by using the present TFD model are compared to the corresponding TFD curves obtained from 3-D FEA results for the static contact problem between two identical aluminum spheres. Finite element analyses are performed for the loading history shown in Fig. 8 and Table 1.

The mechanical properties of the aluminum sphere are: Young's modulus $E = 7.0 \times 10^{10}$ N/m^2, Poisson's ratio $v = 0.3$, material yield stress $\sigma_Y = 1.0 \times 10^8 4$ N/m^2, and coefficient of friction between the sphere and the

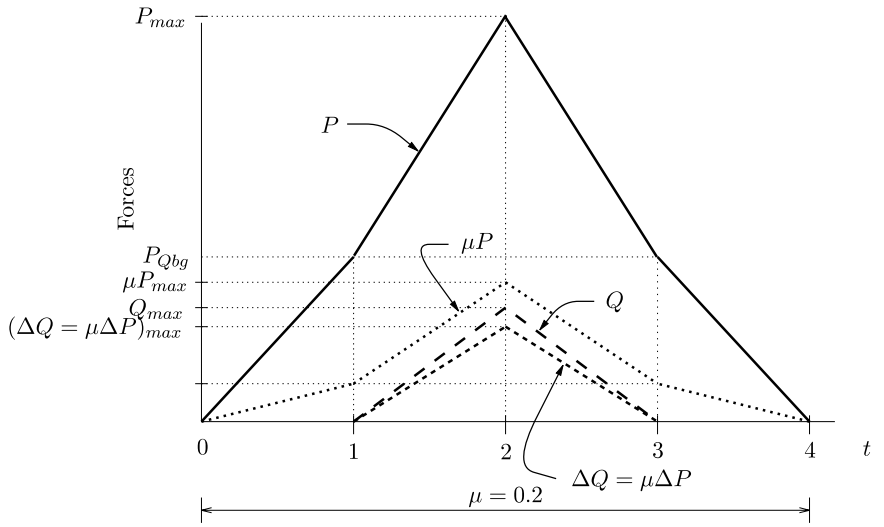

Fig. 8. Loading history for the comparison of TFD curves.

Table 1
Force parameters for loading history shown in Fig. 8

Loading history	$P_{\max}(N)$	$Q_{\max}(N)$	$P_{\mathrm{Qbg}}(N)$	$\mu P_{\max}(N)$
$\mathbb{A}$	1500	270	300	300
$\mathbb{B}$	500	90	100	100
$\mathbb{C}$	250	45	50	50
$\mathbb{D}$	2600	500	2600	520

planar surface $\mu = 0.2$. The radius of the aluminum sphere is $R = 0.1$ m. For the FEA, elastic-perfectly-plastic and time-independent plasticity are employed. For the purpose of comparison, only some of the TFD curves are presented in this paper, and we refer the interested readers to [31] for more details on the related FEA models and results.

The TFD curves shown in Fig. 9 are produced using the following procedures: At first, we use the loading history $\mathbb{A}$ (shown in Fig. 8 and Table 1) as the input for the FEA using ABAQUS with elastic-perfectly-plastic sphere material in the contact problem to compute the time history of the normal displacement denoted by α_{fe} and of the tangential displacement δ_{fe}. Since the TFD model presented in Section 3.2 is of the displacement-driven type, the FEA displacement results α_{fe} and δ_{fe} are used as input into our MATLAB code, which is based on Algorithm 3.1, to compute the tangential force Q_{pm}. The normal force P is calculated using the elasto-plastic NFD model described in [2]. The TFD curve from the MD theory [30] is obtained by inputting the loading history $\mathbb{A}$ (shown in Fig. 8 and Table 1) to obtain the output of tangential displacement history $\delta_{\min}$ for elastic contact. The results with the loading histories $\mathbb{B}$, $\mathbb{C}$, and $\mathbb{D}$ shown in Figs. 10–12, respectively, are produced using a similar procedure.

Remark 4.1. It should be noticed that the FD relationship shown in Figs. 9–12 are produced using procedures that are different in nature. That is, the FD curves from the FEA results are produced using a force-driven procedure, while the FD curves from the proposed elasto-plastic TFD model are produced using a displacement-driven procedure. Since at the beginning we do not know the time history of the tangential displacement, we use FEA to produce such time history using a force-driven procedure, in which the time history of P and Q is given. The time history of the tangential displacement obtained from FEA is then used as input for the present TFD model to obtain the time history of the tangential force in a displacement-driven procedure. The results from the MD theory [30] are produced in a force-driven procedure for comparison.

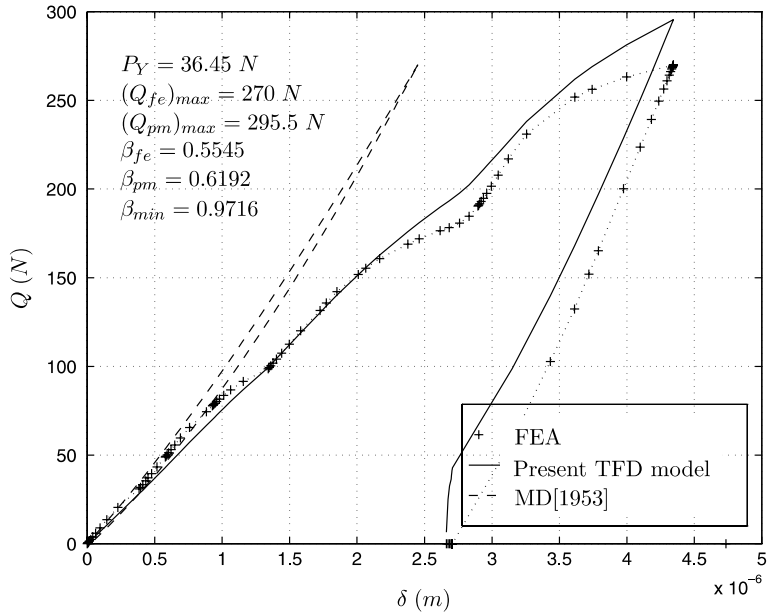

Fig. 9. TFD curves for loading history $\mathbb{A}$ (Fig. 8 and Table 1): Comparison of the present elasto-plastic TFD model, FEA, and Mindlin & Deresiewicz [1953] (MD[1953]) elastic contact theory.

Fig. 9 shows the TFD curves under varying normal force P with $P_{\max} = 1500$ N. It can be seen that the TFD curve produced by the present elasto-plastic TFD model agrees with the TFD curve from FEA results. Since $P_{\max} = 1500\ \text{N} > P_Y = 36.45\ \text{N}$, both the curve from FEA results and the curve from the present TFD model show much larger energy dissipation in the tangential direction than the TFD curve from the MD theory [30] for elastic contact. Clearly, the MD theory [30] cannot predict the TFD relationship correctly for elasto-plastic contact when there is plastic deformation. Quantitatively, the maximum tangential force employed in FEA is $(Q_{fe})_{\max} = 270$ N, which is part of the time history of the applied forces that produce the time history of tangential displacement used as input for the present TFD model. In this fashion, the maximum tangential force produced from the present TFD model is $(Q_{pm})_{\max} = 295.5$ N, which differs from $(Q_{fe})_{\max}$ by 9.4%. There is very good overall agreement between the TFD curve from FEA and the TFD curve from the present TFD model as shown in Fig. 9. It is noted that even the step-like behavior during the loading stage is reproduced by the present TFD model. We emphasize that there is thus far no TFD model in the literature that exist for elasto-plastic contact, while existing TFD model for elastic contact cannot achieve the overall quality shown in Fig. 9. The coefficient of restitution β for tangential direction represents the energy dissipation ratio in the tangential direction of the contact, which is computed by taking the square root of the ratio between the restoring energy (area under the unloading curve) and the storing energy (area under the loading curve) in tangential direction, i.e.,

$$\beta := \left(\frac{\text{Area under tangential unloading curve}}{\text{Area under tangential loading curve}}\right)^{1/2} = \left(\frac{\sum_{i\in\{\delta_i-\delta_{i-1}>0\}}^{\text{loading}} \frac{1}{2}(\delta_i-\delta_{i-1})(Q_i+Q_{i+1})}{\sum_{j\in\{\delta_j-\delta_{j-1}<0\}}^{\text{unloading}} -\frac{1}{2}(\delta_j-\delta_{j-1})(Q_j+Q_{j+1})}\right)^{1/2}. \tag{4.1}$$

Fig. 9 shows the tangential coefficient of restitution from the present TFD model is $\beta_{pm} = 0.6192$, which differs from the FEA result, $\beta_{fe} = 0.5545$, by 11.7%. Both β_{pm} and β_{fe} are much smaller than the coefficient $\beta_{\min} = 0.9716$ from the MD theory [30].

Fig. 10 shows the TFD curves under varying normal force P with $P_{\max} = 500$ N (loading history $\mathbb{B}$ in Fig. 8 and Table 1). The TFD curve produced by the present elasto-plastic TFD model is close to the TFD curve from FEA, especially for the loading part. Since $P_{\max} = 500\ \text{N} > P_Y = 36.45\ \text{N}$, both the TFD curve from FEA and the TFD curve produced by the present TFD model show much larger energy dissipations in tan-

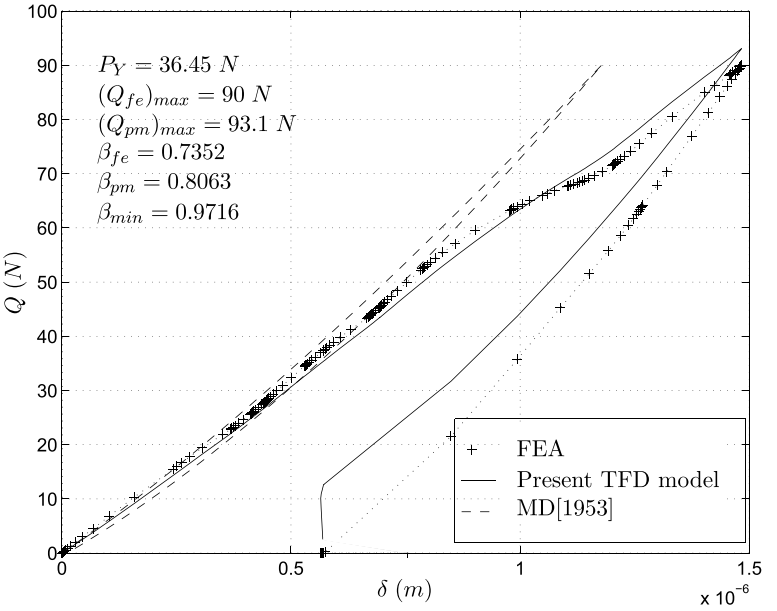

Fig. 10. TFD curves for loading history $\mathbb{B}$ (Fig. 8 and Table 1): Comparison of the present elasto-plastic TFD model, FEA, and Mindlin & Deresiewicz [1953] (MD[1953]) elastic contact theory.

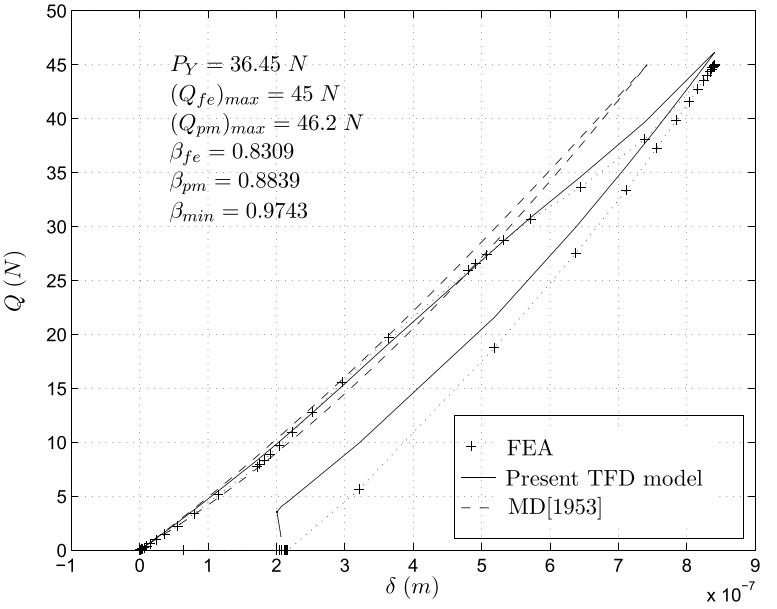

Fig. 11. TFD curves for loading history $\mathbb{C}$ (Fig. 8 and Table 1): Comparison of the present elasto-plastic TFD model, FEA, and Mindlin & Deresiewicz [1953] (MD[1953]) elastic contact theory.

gential direction than that from the MD theory [30] for elastic contact. Again, Fig. 10 shows that the MD theory [30] cannot predict the TFD relationship correctly for elasto-plastic contact when there is plastic deformation. On the other hand, the maximum tangential force used for the FEA is $(Q_{fe})_{\max} = 90$ N, and the maximum tangential force produced from the present TFD model is $(Q_{pm})_{\max} = 93.1$ N, i.e., a difference of only 3.4%. The tangential coefficient of restitution from the present TFD model, $\beta_{pm} = 0.8063$, differs from that of FEA results, $\beta_{fe} = 0.7352$, by only 9.7%. Both β_{pm} and β_{fe} are sharply different from $\beta_{\min} = 0.9716$ from

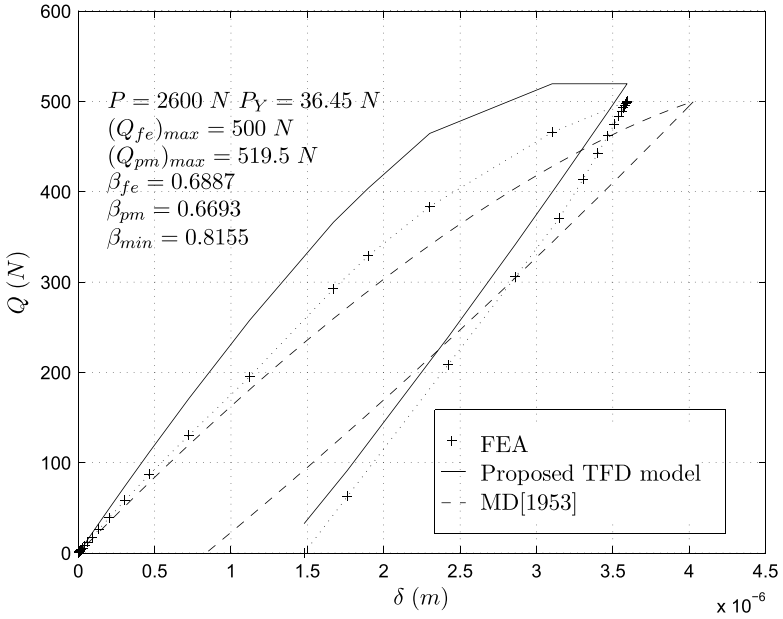

Fig. 12. TFD curves for loading history $\mathbb{D}$ (Fig. 8 and Table 1): Comparison of the present elasto-plastic TFD model, FEA, and Mindlin & Deresiewicz [1953] (MD[1953]) elastic contact theory.

the MD theory [30]. The present elasto-plastic TFD model correctly predicts not only the tangential force level, but also the energy dissipation of this elasto-plastic contact in tangential direction.

Fig. 11 is one more example showing the comparison of TFD curves under varying normal forces, and computed using different models. In this case, the maximum normal force is $P_{\max} = 250$ N (the loading history $\mathbb{C}$ in Fig. 8 and Table 1). It shows again that the TFD curve produced by the present elasto-plastic TFD model is close to the TFD curve from FEA, with both of those TFD curves for elasto-plastic contact being quite different from the TFD curve produced by the MD theory [30] for elastic contact. The maximum tangential force used for the FEA is $(Q_{fe})_{\max} = 45$ N, and the maximum tangential force produced from the present TFD model is $(Q_{pm})_{\max} = 46.2$ N, i.e., a difference of only 2.6%. The tangential coefficient of restitution from different models are: $\beta_{fe} = 0.8309$, $\beta_{pm} = 0.8839$, and $\beta_{\min} = 0.9743$.

Fig. 12 is an example showing the comparison of TFD curves under a varying tangential force Q and a constant normal force $P = 2600$ N (the loading history $\mathbb{D}$ in Fig. 8 and Table 1). As described in Section 3.1, we can see in Fig. 12 that the TFD curve from FEA with the effect of plastic deformation ($P = 2600\ \text{N} \gg P_Y = 36.45$ N) is stiffer in the early loading stage than that from the MD theory [30] for elastic contact. Fig. 12 also shows that the energy dissipation in the tangential direction from FEA is larger than that from the MD theory [30], because energy dissipation caused by plastic deformation is accounted for in FEA while only the energy dissipation caused by friction is accounted for in the MD theory [30]. The TFD curve produced by the present elasto-plastic TFD model (Fig. 12) agrees qualitatively incorporate the stiffening effect that discussed in Section 3.1. After an overshoot in the stiffening effect at the beginning of the loading stage, the present model softens to an accurate value for the maximum tangential force (probably caused by the friction limit), and then follows an unloading curve with the same slope as in FEA (which is also stiffer than the TFD curve from the MD elastic contact theory [30]). Thus despite a decrease in accuracy in the loading stage due to excessive normal load P, the present TFD model shows good recovery of the stiffness overshoot and accuracy in the unloading stage. In addition, Fig. 12 shows that the tangential coefficient of restitution from the present TFD model, $\beta_{pm} = 0.6693$, agrees with the FEA results, $\beta_{fe} = 0.6887$, with a difference of only 2.8%.

Remark 4.2. From the results shown in Figs. 9–12, we observe the following behavior of the present elasto-plastic TFD model: (i) For the case where both P and Q are varying, the results produced by the present TFD

model are quantitatively accurate in both the force magnitude and the dissipation of the energy in comparison with FEA results. (ii) For the case where $P = constant$ ($\frac{|\Delta Q|}{|\Delta P|} = \infty$) and $P \gg P_Y$, there is a substantially larger amount of plastic deformation and contact area, the present TFD model displays some stiffness overshoot at the beginning of the loading stage, but a good maximum tangential force and a good unloading curve.

5. Conclusion

We have presented an elasto-plastic frictional tangential force–displacement (TFD) model for two colliding spheres in a displacement-driven version that is needed for implementation in DEM simulation codes. The present TFD model accounts for both elastic and plastic deformations that inevitably occur in most impact problems. A cardinal feature of the present TFD model is the additive decomposition of the contact radius into an elastic part and a plastic correction part, similar to the additive decomposition of the elasto-plastic strain in the continuum theory of elastoplasticity. The effect of permanent indentation after impact is represented by a correction to the radius of curvature. The effect of material softening due to plastic flow is represented by a correction to the elastic moduli. To account for the effect of the change in the normal force P on the TFD relationship, a similar procedure as that developed in [32] for elastic contact is employed. Thus, the present elasto-plastic TFD model is easy to implement, and is suitable for DEM simulation of systems involving a large number of particles. The present elasto-plastic frictional TFD model, together with the elasto-plastic normal force–displacement (NFD) model in [2], form a set of elasto-plastic force–displacement (FD) models that are consistent with each other. For simulation of granular flows by DEM, there has been a lack of a force–displacement model that is completely consistent in both the normal direction and in the tangential direction and that accounts for plastic deformation. Numerical examples show that the present elasto-plastic frictional TFD model produces accurate results in both the tangential force level and the energy dissipation (the area inside the hysteretic TFD curves) for a wide range of loading cases. More details on the application of the present elasto-plastic NFD and TFD models in DEM simulations will be presented in the future.

Acknowledgments

We thank Lee Lesburg for his discussions on the formulation and the finite element analyses. We acknowledge the support from the National Science Foundation.

References

[1] L. Vu-Quoc, L. Lesburg, X. Zhang, An accurate tangential force–displacement model for granular-flow simulations: Contacting spheres with plastic deformation, force-driven formulation, Journal of Computational Physics 196 (1) (2004) 298–326.
[2] L. Vu-Quoc, X. Zhang, An elasto-plastic contact force–displacement model in the normal direction: displacement-driven version, Proceedings of the Royal Society of London Series A 455 (1991) 4013–4044.
[3] G.M. Smith, T.R. Davies, M.J. McSaveney, D.H. Bell, The Acheron rock avalanche Canterbury, New Zealand – morphology and dynamics, Landslides 3 (1) (2006) 62–72.
[4] K. Kelfoun, T.H. Druitt, Numerical modeling of the emplacement of Socompa rock avalanche, Chile, Journal of Geophysical Research-Solid Earth 110 (B12) (2005), article no.B12202.
[5] M. Barbolini, A. Biancardi, F. Cappabianca, L. Natale, M. Pagliardi, Laboratory study of erosion processes in snow avalanches, Cold Regions Science and Technology 43 (1-2) (2005) 1–9.
[6] E. Lajeunesse, C. Quantin, P. Allemand, C. Delacourt, New insights on the runout of large landslides in the Valles-Marineris canyons, Mars, Geophysical Research Letters 33 (4) (2006), article no.L04403.
[7] P. Salatino, Assessment of motion-induced fluidization of dense pyroclastic gravity currents, Annals of Geophysics 48 (4–5) (2005) 843–852.
[8] C. Cassar, M. Nicolas, O. Pouliquen, Submarine granular flows down inclined planes, Physics of Fluids 17 (10) (2005), article no.103301.
[9] T. Mullin, Mixing and de-mixing, Science 295 (5561) (2002) 1851.
[10] K. Chang, Secrets of the singing sand dunes, New York Times, 2006. Tue, 25 Jul, Science-Times section, p.F1. Web address: nytimes.com/science.
[11] C. Holden, Sands sing for France, Science 300 (2003) 47.
[12] B. Andreotti, The song of dunes as a wave-particle mode locking, Physical Review Letters 93 (23) (2004), article no.238001.

[13] S. Douady, A. Manning, P. Hersen, H. Elbelrhiti, S. Protiere, A. Daerr, B. Kabbachi, Song of the dunes as a self-synchronized instrument, Physical Review Letters 97 (1) (2006), article no.018002.
[14] P. Jop, Y. Forterre, O. Pouliquen, A constitutive law for dense granular flows, Nature 441 (Jun) (2006) 727–730.
[15] L. Vu-Quoc, X. Zhang, O.R. Walton, 3-D discrete-element method for dry granular flows of ellipsoidal particles, Computer Methods in Applied Mechanics and Engineering 187 (3) (2000) 483–528.
[16] M.A.I. Schutyser, W.J. Briels, A. Rinzema, R.M. Boom, Numerical simulation and PEPT measurements of a 3D conical helical-blade mixer: a high potential solids mixer for solid-state fermentation, Biotechnology and Bioengineering 84 (1) (2003) 29–39, Oct 5.
[17] O. Hlungwani, J. Rikhotso, H. Dong, M.H. Moys, Further validation of DEM modeling of milling: effects of liner profile and mill speed, Minerals Engineering 16 (10) (2003) 993–998.
[18] E. Tijskens, H. Ramon, J. De Baerdemaeker, Discrete element modelling for process simulation in agriculture, Journal of Sound and Vibration 266 (3) (2003) 493–514, Sep 18.
[19] E. Dintwa, M. Van Zeebroeck, E. Tijskens, H. Ramon, Determination of parameters of a tangential contact force model for viscoelastic spheroids (fruits) using a rheometer device, Biosystems Engineering 91 (3) (2005) 321–327.
[20] A. Di Renzo, F.P. Di Maio, Comparison of contact-force models for the simulation of collisions in DEM-based granular flow codes, Chemical Engineering Science 59 (3) (2004) 525–541.
[21] A.O. Raji, J.F. Favier, Model for the deformation in agricultural and food particulate materials under bulk compressive loading using discrete element method. I: Theory, model development and validation, Journal of Food Engineering 64 (3) (2004) 359–371.
[22] N. Fillot, I. Iordanoff, Y. Berthier, A granular dynamic model for the degradation of material, Journal of Tribology – Transactions of the ASME 126 (3) (2004) 606–614.
[23] K. Harstad, J. Bellan, On possible release of microbe-containing particulates from a Mars lander spacecraft, Planetary and Space Science 54 (3) (2006) 273–286.
[24] X. Zhang, L. Vu-Quoc, Modeling the dependence of the coefficient of restitution on the impact velocity in elasto-plastic collisions, International Journal of Impact Engineering 27 (3) (2002) 317–341.
[25] X. Zhang, L. Vu-Quoc, Simulation of chute flow of soybeans using an improved tangential force–displacement model, Mechanics of Materials 32 (2) (2000) 115–129.
[26] L. Vu-Quoc, X. Zhang, L. Lesburg, A normal force–displacement model for contacting spheres accounting for plastic deformation: force-driven formulation, Journal of Applied Mechanics – Transactions of the ASME 67 (2) (2000) 363–371.
[27] G. Plantard, M. Papini, Mechanical and electrical behaviors of polymer particles. Experimental study of the contact area between two particles. Experimental validation of a numerical model, Granular Matter 7 (1) (2005) 1–12.
[28] H. Hertz, Über die Berührung fester elastischer Körper (on the contact of elastic solids), Journal fur die Reine und Angewandte Mathematik 92 (1882) 156–171.
[29] K.L. Johnson, Contact Mechanics, second ed., Cambridge University Press, New York, 1985.
[30] R.D. Mindlin, H. Deresiewicz, Elastic spheres in contact under varying oblique forces, ASME Journal of Applied Mechanics 20 (September) (1953) 327–344.
[31] L. Vu-Quoc, X. Zhang, L. Lesburg, Normal and tangential force–displacement relations for frictional elasto-plastic contact of spheres, International Journal of Solids and Structures 38 (36-37) (2001) 6455–6489.
[32] L. Vu-Quoc, X. Zhang, An accurate and efficient tangential force–displacement model for elastic-frictional contact in particle-flow simulations, Mechanics of Materials 31 (1999) 235–269.
[33] J. Jager, Some comments on recent generalizations of Cattaneo–Mindlin, International Journal of Solids and Structures 38 (14) (2001) 2453–2457.
[34] J. Jager, New analytical and numerical results for two-dimensional contact profiles, International Journal of Solids and Structures 39 (4) (2002) 959–972.
[35] Otis R. Walton, Robert L. Braun, Viscosity, granular-temperature and stress calculations for shearing assemblies of inelastic, frictional disks, Journal of Rheology 30 (5) (1986) 949–980.
[36] Otis R. Walton, Numerical simulation of inelastic frictional particle–particle interactions, in: M.C. Roco (Ed.), Particulate Two-Phase Flow, Butterworth–Heinemann, Stoneham, MA, 1993, pp. 884–911 (Chapter 25).
[37] Charles E. Smith, Pao-Pao Liu, Coefficients of restitution, ASME Journal of Applied Mechanics 59 (1992) 963–969.
[38] Kh.F. Kangur, I.R. Kleis, Experimental and theoretical determination of the coefficient of velocity restitution upon impact, Mechanics of Solids 23 (5) (1988) 182–185.
[39] W. Goldsmith, Impact: The Theory and Physical Behaviour of Colliding Solids, Edward Arnold Ltd., London, 1960.
[40] X. Zhang, L. Vu-Quoc, A method to extract the mechanical properties of particles in collision based on a new elasto-plastic normal force–displacement model, Mechanics of Materials 34 (12) (2002) 779–794.